IOPscience iopscience.iop.org

Home Search Collections Journals About Contact us My IOPscience

The chemical structure of rare earth superlattices: a high-resolution x-ray scattering study

This article has been downloaded from IOPscience. Please scroll down to see the full text article.

1996 J. Phys.: Condens. Matter 8 6553

(http://iopscience.iop.org/0953-8984/8/36/008)

View the table of contents for this issue, or go to the journal homepage for more

Download details:
IP Address: 171.66.16.206
The article was downloaded on 13/05/2010 at 18:36

Please note that terms and conditions apply.

J. Phys.: Condens. Matter **8** (1996) 6553–6567. Printed in the UK

The chemical structure of rare earth superlattices: a high-resolution x-ray scattering study

D F McMorrow†, P P Swaddling, R A Cowley, R C C Ward and M R Wells
Oxford Physics, Clarendon Laboratory, Parks Road, Oxford, UK

Received 11 January 1996, in final form 13 May 1996

Abstract. The chemical structure of a series of Ho/Lu and Ho/Y superlattices, all grown by MBE, has been investigated using high-resolution x-ray scattering techniques. The detailed functional form of the scattering was determined in scans performed both parallel and perpendicular to the growth direction. For scans of the wave-vector transfer parallel to the growth direction the superlattice satellites broaden as a function of the satellite index. This is shown to be consistent with the presence of discrete cumulative roughness in the superlattices that scales with the thickness of the superlattice period. The transverse width of the superlattice Bragg peaks broadens almost linearly as a function of the component of the reduced wave-vector parallel to the growth direction, while the line shape is invariant, and is described by a Lorentzian raised to the power of ≈5/2. It is shown that this arises from the conformal nature of the interface roughness, and the roughness exponent characterizing the *average* interface is determined to be $\alpha = 0.85 \pm 0.05$. The dependence of the interface morphology on the growth temperature is also considered, and the limitations of current structural models discussed.

1. Introduction

Advanced deposition techniques are being used to produce an increasing range of artificial structures, either in the form of thin films or superlattices. For example, molecular beam epitaxy (MBE) was originally developed to fabricate semiconductor heterostructures, but is now being used to produce metals, insulators and even mixed systems [1]. Its great utility results from the relative ease with which it is possible to control the deposition rate and substrate temperature. These determine the balance between fluctuations due to the stochastic nature of the incident beam and surface diffusion, and hence the growth morphology. In spite of this control it is often difficult to achieve perfect layer-by-layer growth, and instead a rough surface is obtained.

The roughness in a superlattice may be divided for convenience into four types as indicated in figure 1 (see, for example, Fullerton *et al* [2]). Conformal roughness results when there is uniform growth across the whole sample so that the deviation from the average flat interface is determined by the roughness of the substrate, and this roughness propagates through the entire thickness of the layer. The other extreme is conformal cumulative roughness where the surface mobility of the incident atoms is so restricted that the width of successive interfaces increases. In between, the growth conditions may be such as to produce uncorrelated or partially correlated roughness. Here the surface mobility is high enough to keep the interfacial width constant, but too low to form flat interfaces.

† Present address: Department of Solid State Physics, Risø National Laboratory, DK-4000 Roskilde, Denmark.

0953-8984/96/366553+15$19.50 © 1996 IOP Publishing Ltd

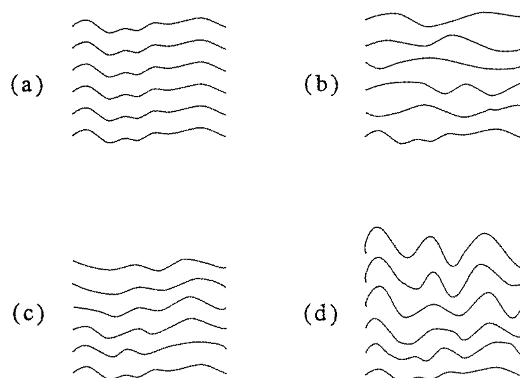

Figure 1. The four possible types of roughness found in a superlattice: (a) conformal, (b) uncorrelated, (c) partially conformal and (d) cumulative, partially conformal.

It is now well established that interface states, and more generally the morphology of the interface, have a deterministic influence on the physical properties of superlattices. For example, there is considerable current interest in the mechanisms by which interfacial roughness modifies the giant magneto-resistance signal found in some transition metal superlattices [3, 4]. In addition there is obviously the intrinsic interest in understanding the growth modes of superlattice systems, and in particular relating the results of diffraction measurements to models of rough surfaces. A dynamic scaling relation has been proposed for such surfaces, characterized by two exponents α and β that describe the spatial and temporal evolution of the roughness [5]. Considerable theoretical effort has been devoted to determining the values of these exponents for different growth models, and there have now been many experimental investigations of a diverse range of systems. Although studies using both electron and neutron diffraction have made significant contributions to this field, x-ray scattering is probably the best non-destructive technique for characterizing the structure of superlattices.

In this paper we present the results of a high-resolution x-ray scattering study of a series of rare-earth superlattices grown by MBE. Previous investigations of these materials were mostly restricted to low-resolution experiments, which are unable to distinguish between the types of roughness shown in figure 1, and instead were interpreted using simple interdiffusional models [6]. We shall show that our experiments performed at higher resolution, combined with more sophisticated modelling techniques, reveal a more complete picture of the microscopic structure of the superlattices. In addition, by studying a series of nominally identical samples grown at different substrate temperatures we are able to determine the dependence of the growth morphology on substrate temperature. The layout of the paper is a follows. In section 2 a brief review is given of models of scattering from superlattices. The experimental details are presented on section 3, and the experimental results described in section 4. The systematic trends revealed by fitting the data are then considered in section 5, where the limitations of the current models are also discussed. Finally the results are summarized in section 6. We note that some of the work presented in this paper has been reported previously [7].

2. Models of disorder in superlattices

Over the last decade structural models of disorder in superlattices have become ever more sophisticated. Up to the mid-eighties, most models assumed that the disorder was due to inter-diffusion at the interfaces [6, 8]. In a diffraction experiment the key signature of chemical disorder in a superlattice is that the intensity of the satellite peaks, measured in a longitudinal scan of the x-ray wave-vector transfer, $\boldsymbol{Q}$, i.e. parallel to the growth direction, fall off more rapidly than calculated for an an ideal square wave composition profile. If the disorder arises solely from chemical interdiffusion or steps at the interfaces, while the superlattice period remains constant, then the effect is to reduce the intensity of the satellites without any broadening. Various functions have been assumed for the rounding of the compositional profile at the interface between the constituents, including damped square wave or trapezoidal forms [6, 8]. These models were then compared with data, and an effective interface width and average lattice parameters were extracted. This approach proved to give an adequate description of many systems, and it was only in the second half of the decade when high-resolution x-ray scattering measurements became more routine that a need was found for a more complete picture.

To date the most elegant model for the longitudinal scattering that goes beyond the simple inter-diffusional picture is due to Fullerton and co-workers [9]. The key assumption of their kinematical model is that the longitudinal scattering, $I(Q)$, may be expressed as an ensemble average over all possible statistically independent one-dimensional superlattice structures. (In other words the interfaces are assumed to be flat.) Further, the number of layers of each constituent are described by Gaussian distributions around mean values of N_A and N_B with variances ω_A and ω_B. With these assumptions, an expression for $I(Q)$ was derived in closed form that describes the scattering from a system with discrete cumulative disorder produced by fluctuations in the number of lattice planes. The disorder is viewed as discrete in the sense that the number of lattice planes is assumed to an integer. A second ingredient in their model, is to assume that the lattice parameter at an interface is continuously distributed about a mean value with variance δ, so that it has an normal distribution of FWHM $\approx 2.35\delta$. The discrete cumulative disorder produces a broadening of the satellite peaks that increases with the satellite index, whereas the effect of the continuous disorder in the interface lattice parameter is to broaden all peaks by the same amount. This model has now been applied successfully to several systems, including Mo/Ni and Nb/Cu [9], but it does not include the effects of any correlations in the roughness of the interfaces.

The signature in a diffraction experiment of significant transverse correlations in the interface roughness is the existence of a finite width to the scattering in the transverse direction. The functional form of the scattering from rough surfaces has been derived by several authors. The starting point of these derivations is a consideration of the scaling relations that have been proposed to apply to the growth of a rough surface. In the late-time regime, the dynamic scaling form of the equal-time height–height correlation function $G(r)$ describing a rough surface of area L^2 is given by [5]

$$\begin{aligned} G(r) &= \langle [h(r) - h(0)]^2 \rangle \\ &= \begin{cases} Ar^{2\alpha} & \text{for } r \ll L \\ h_0 & \text{for } r \gg L \end{cases} \end{aligned} \tag{1}$$

where $h(r)$ describes the height of the surface as a function of the in-plane position r, $\langle \ldots \rangle$ denotes an ensemble average, and A and h_0 are constants. The scattering then consists of a specular part that arises from the part of the integral for $r \gg L$, and a diffuse or

non-specular part which may be written as [10, 11]

$$I(\mathbf{p}, q) \propto \int_0^\infty r \exp(-Aq^2 r^{2\alpha}/2) J_0(pr) \mathrm{d}r \tag{2}$$

where we have assumed that L is sufficiently large that it is effectively infinite. Here J_0 is zeroth-order Bessel function, and we write the reduced x-ray wave-vector transfer relative to the main Bragg peak as (p_x, p_y, q), with $\mathbf{p}$ in the plane of the film and q perpendicular to the surface.

The integral in equation 2 can only be evaluated analytically for two values of the exponent α: if $\alpha = 1/2$, then the transverse line shape is a Lorentzian to the power of 3/2, with a width that varies quadratically with q, while $\alpha = 1$ yields a Gaussian line shape and a width that vary linearly with q. As the value of α is increased from 1/2, the line shape can be described as a Lorentzian raised to successively higher powers. Thus, in principle by measuring how the x-ray scattering evolves as a function of $\mathbf{p}$ and q it is possible to determine the roughness exponent α. In practice it may be difficult to distinguish between the specular and non-specular parts of the scattering. This is particularly the case if the sample has a mosaic spread as indeed is the case with our samples. It is then more appropriate to analyse the data by integrating the intensity over the transverse p component to obtain the intensity for each longitudinal q. This can then be analysed in the same way as the specular intensity except that the resulting interface width has a different interpretation. For the truly specular scattering the width is obtained from the chemical density distribution averaged over all r, whereas for the integrated intensity the width is obtained for each r and then averaged. If the interface has a chemical diffusion width and also wanders (in the sense that there is correlated roughness) as a function of r, then the interface width obtained from the specular scattering is the sum of both effects, while the interface width obtained from the integrated intensity depends on the chemical diffusion only. This difference is clearly seen if L in equation (1) becomes very large. The specular intensity is then greatly reduced because the effect of the roughness becomes very large, but the non-specular part is well defined and can be analysed to give the parameters A and α.

These arguments have been developed for a surface, but can be generalized to include the interfaces [12, 13] between the two constituents forming a superlattice. If the roughness of the interfaces is conformal, then the diffuse or non-specular scattering peaks at the longitudinal wave-vectors q corresponding to the superlattice peaks. Analysis of this scattering then gives a measure of the conformal component of the interface roughness. This is the part measured in the experiments described below. Roughness of the interfaces which is not correlated gives rise to diffuse scattering which varies slowly with q. In practice it is very difficult to separate this weak scattering from the background and so we have been unable to measure the uncorrelated roughness. In addition to the exponent α that describes the spatial correlations of the roughness, the temporal growth of a rough surface is also characterized by another exponent β [5], such that the saturated value of the rms width is proportional to t^β. As we could not determine the value of β in our measurements, we shall not consider it further.

There exist two distinct categories of model that have been developed to describe the growth process. In the first, it is assumed that relaxation mechanisms, such as surface diffusion, are sufficient to prevent the formation of voids and overhangs. For this conservative growth mode it has been shown that the roughness exponents, and in particular α, are very sensitive to the local rules governing the relaxation, with typical values in $d = 2 + 1$ dimensions spanning the range from $\alpha = 2/3$ [14] to $\alpha = 0.95$ [15]. In contrast, non-conservative growth models are believed to belong to the single KPZ

universality class [16], which for $d = 2+1$ predicts that $\alpha = 1/3$. (Here the lower value of α simply reflects the fact that in the absence of strong relaxation processes a more jagged surface is likely to form.) There is still some controversy [17–20] over which, if either, of the above growth modes correctly describes MBE, and this provided part of the motivation for our study.

The value of the exponent α has been determined for several different systems using a variety of probes. Atomic force microscopy measurements on electrodeposited Cu produced the value $\alpha = 0.87 \pm 0.05$ [21], while the same technique applied to the deposition of CuCl on CaF_2 by MBE gave the result $\alpha = 0.84 \pm 0.05$ [22]. X-ray reflectivity has also been used to study a number of metallic systems, and these include: Co/Pt superlattices, $\alpha = 0.65 \pm 0.03$ [23]; thermally deposited Au and Ag on polished quartz, $\alpha = 0.46 - 0.95$ [24]; vapour deposited Ag on Si, $\alpha = 0.70 \pm 0.10$ [25]. Other non-metallic systems investigated using low-angle x-ray scattering include liquid-crystal polymers and semiconductor superlattices, with exponents of $\alpha = 0.25 \pm 0.05$ [26] and $\alpha = 0.4$ [27] respectively. Thin films of Fe have also been studied both in deposition using electron diffraction, $\alpha = 0.79 \pm 0.05$ [28], and for erosion using scanning tunnelling microscopy, $\alpha = 0.53 \pm 0.02$ [29], when the erosion was produced by ion-beam bombardment.

3. Experimental details

The rare-earth superlattices were grown in Oxford using MBE, and were originally produced for studies of their magnetic properties. Following the technique developed by Kwo *et al* [30], the rare-earth metals were deposited on a Nb buffer layer grown on a sapphire substrate (see [31, 32] for more details). It is known from earlier work [30] that the rare-earths retain their *hcp* crystal structure and grow as single crystals. The epitaxial relationships in the growth direction are: $(110)Al_2O_3 \parallel (110)$ Nb $\parallel$ (001) rare earth. A schematic representation of a rare-earth superlattice is given in figure 2. In table 1 we list their average structural parameters, where we have used the notation $(Ho_{N_A}/R_{N_B})_M$, with N_A and N_B the number of atomic planes, M is the number of bi-layers and R = Y or Lu. All of the superlattices listed in table 1 were grown at a nominal substrate temperature of 400 °C. To allow us to investigate any dependence of the interface roughness on substrate temperature, a series of three superlattices with nominal composition $(Ho_{40}/Y_{15})_{15}$ were produced sequentially with substrate temperatures of 250, 400 and 600 °C.

The x-ray scattering experiments were performed mainly using a triple-crystal x-ray diffractometer in the Clarendon Laboratory, Oxford University. This instrument is located on a 6 kW rotating-anode source, and Ge (111) crystals are used to both monochromate the incident radiation (λ = 1.541 Å) and to analyse the scattered beam. Additional measurements were also made using a four-circle (λ = 1.546) diffractometer on beam line X22B at NSLS, Brookhaven National Laboratory. In both cases the resolution in the scattering plane was typically 0.001 Å^{-1}, which is much smaller than the scale in wave-vector over which the intensity varies. Consequently it was not necessary to make resolution corrections for the in-plane resolution function. The out-of-plane resolution was worse by a factor of approximately one hundred. This ensured that the intensity was always integrated over this direction, and in the analysis corrections were applied for this component of the resolution function.

The x-ray experiments were performed in two ways. In the first series of experiments the detailed form of integrated scattering parallel to the growth direction was determined. This was achieved by varying the component of the wave-vector transfer parallel to the growth direction, $\boldsymbol{Q}_{para}([00\ell])$, in a step-wise manner through the (002) Bragg peak, and at

Table 1. The structural parameters of the Ho/Lu and Ho/Y superlattices obtained from fitting the model described in the text to data taken in longitudinal scans of the wave-vector transfer. Key: N_A, N_B ω_A, ω_B, and σ are expressed in the number of atomic planes; A = Ho, B = Lu or Y. Note: N_A and N_B are expressed as the mean number of planes.

Sample	N_A	N_B	d_A (Å)	d_B (Å)	ω_A	ω_B	δ (Å)	σ
$(Ho/Lu)_{50}$	43.9	15.8	2.816	2.752	3.4	2.4	0.055	4.3
$(Ho/Lu)_{50}$	20.0	16.7	2.817	2.758	1.3	2.2	0.098	2.3
$(Ho/Lu)_{75}$	8.0	18.2	2.830	2.763	1.0	2.2	0.088	2.4
$(Ho/Lu)_{50}$	18.0	9.5	2.816	2.749	2.8	1.3	0.055	3.8
$(Ho/Lu)_{32}$	11.9	34.0	2.827	2.765	2.2	3.3	0.079	2.1
$(Ho/Lu)_{50}$	17.7	4.7	2.814	2.741	2.2	1.4	0.058	2.2
$(Ho/Lu)_{50}$	24.0	14.4	2.813	2.757	2.8	1.5	0.075	2.7
$(Ho/Y)_{50}$	16.0	61.0	2.771	2.874	2.6	2.5	0.086	4.1
$(Ho/Y)_{30}$	7.8	30.0	2.794	2.872	0.8	1.5	0.080	1.9
$(Ho/Y)_{50}$	39.5	17.0	2.800	2.875	3.3	0.2	0.077	2.6

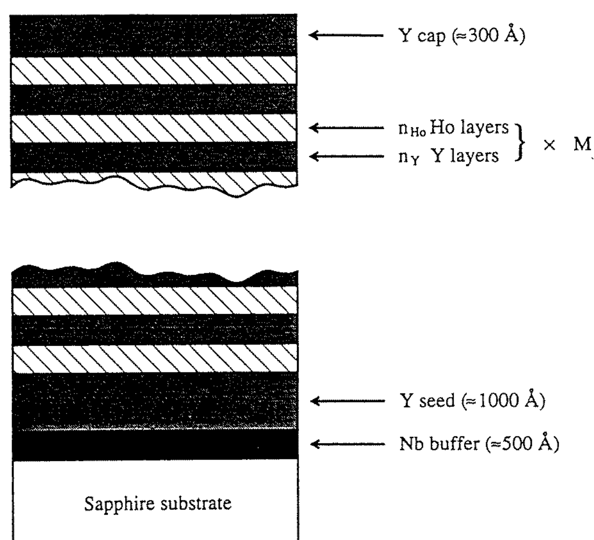

Figure 2. A schematic representation of the ideal structure of a rare-earth superlattice. The epitaxial relationships in the growth direction are: (110) Al_2O_3 ∥ (110) Nb ∥ (001) Rare earth.

each setting of $\boldsymbol{Q}_{para}$ a scan was performed in the transverse direction. Each transverse scan was then integrated, and a background subtraction made to yield the integrated intensity as a function of $\boldsymbol{Q}_{para}$. For some samples, similar measurements were made around (004). We shall refer to data collected by this method as a longitudinal scan. In the second type of experiment the detailed form of the scattering in the transverse direction was investigated. For each of the samples $\boldsymbol{Q}$ was scanned parallel to the growth direction in order to ascertain the exact position of the superlattice satellites. Transverse scans normal to the growth direction, or p_x in the notation of equation (2), were then made through each of the satellites, including a scan through the central peak to determine the sample mosaic

distribution function.

The final set of experiments studied the effect of altering the growth conditions on the interfacial roughness. For these experiments both longitudinal and transverse scans were performed.

An attempt was also made to study the diffuse scattering in the reflectivity at low angles. However, these measurements were dominated by the scattering from the very rough oxide on top of the Y capping layer. As the oxide is polycrystalline, it did not affect our data taken at high angle. Our results therefore illustrate the advantages of using high-angle x-ray scattering to probe interfacial structure.

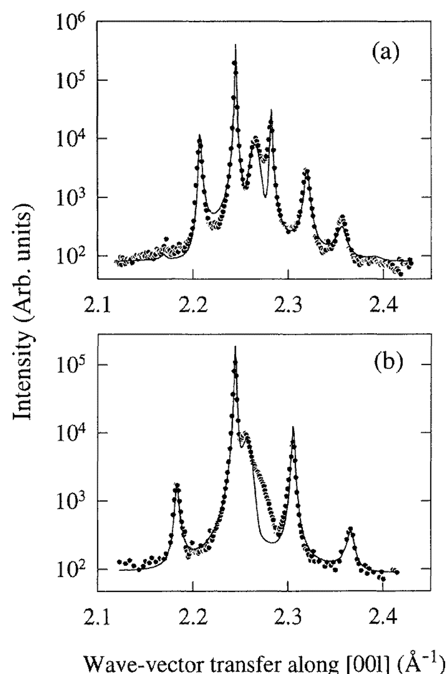

Figure 3. The x-ray scattering from the (a) $(Ho_{44}/Lu_{16})_{50}$ and (b) $(Ho_{20}/Lu_{17})_{50}$ superlattices observed in scans of $\boldsymbol{Q}$ along $[00\ell]$. The intensity at each value of ℓ was integrated by performing a scan normal to the $[00\ell]$ direction, as described in the text. The solid line is a fit to the model described in the text.

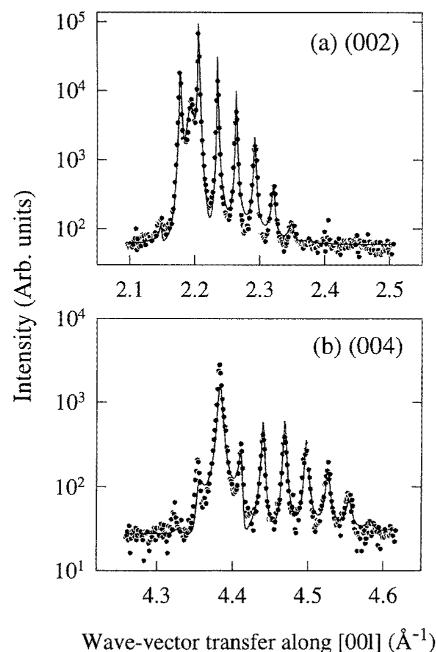

Figure 4. The x-ray scattering from the $(Ho_{16}/Y_{61})_{50}$ superlattice observed in a scan of $\boldsymbol{Q}$ along $[00\ell]$ around (a) the (002) and (b) the (004) Bragg peaks. The solid line is the result of a simultaneous fit of the model to the (002) and (004) data and is described in the text.

4. Results

4.1. Longitudinal scans

Two representative longitudinal data sets are shown in figure 3. The scattering from Ho_{44}/Lu_{16} (top panel) has its most intense peak at $\approx$2.24 Å^{-1}, corresponding to the average lattice spacing of the bi-layer, and a series of equally-spaced superlattice peaks extending out to the third order on the high-Q side, and to second order on the other side. (Here we are using the notation that the nth order satellite is displaced a distance in reciprocal space

$2\pi n/\Delta$ from the most intense peak, where Δ is the superlattice period in Å). In addition there is a broad peak near 2.26 Å^{-1} from the Lu cap and seed layers. The width of the main peak is not resolution limited, but corresponds to a finite structural coherence length of $\approx$ 2000 Å. In addition the width of the superlattice peaks increase with increasing satellite order. These two facts indicate the presence of both discrete and continuous disorder, as defined in section 2. The qualitative features of the data in the bottom panel of figure 3 from Ho_{16}/Lu_{61} are consistent with this picture, and in fact all of the Ho/Lu superlattices investigated displayed the same features. Evidence for coexistence of the two types of disorder were also found in the Ho/Y superlattices, and an example is shown in figure 4, with the main difference being the presence of more superlattice peaks resulting from the higher x-ray contrast between Ho and Y than Ho and Lu.

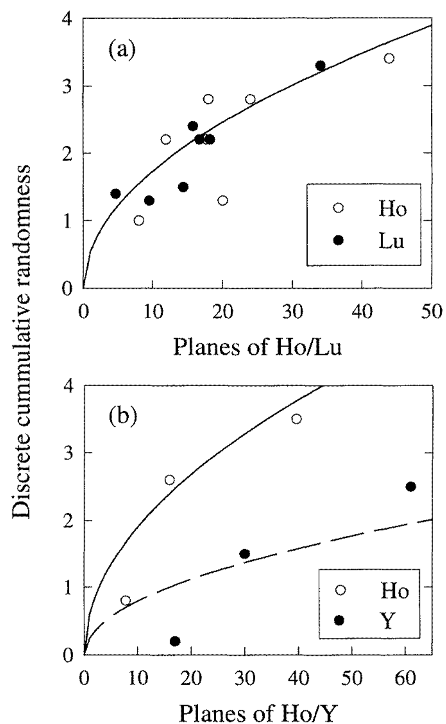

Figure 5. The variance in the number of layers (which is a measure of the discrete cumulative randomness) deduced for the (a) Ho/Lu (open circles Ho, filled circles Lu) and (b) Ho/Y superlattices (open circles Ho, filled circles Y). The lines are best fits to a functional form proportional to the square-root of the number of atomic planes.

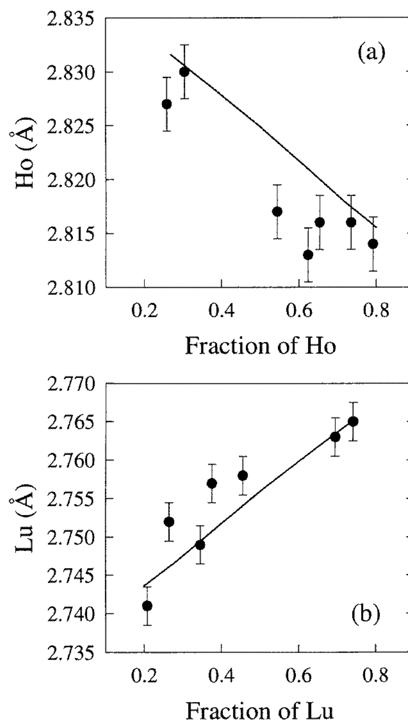

Figure 6. The lattice parameters as a function of the fractional composition (calculated from the number of atomic layers in a bilayer) of the Ho/Lu superlattices, deduced from fitting the scattering model to the $[00\ell]$ scans. The bulk values of the inter-planar spacing $(c/2)$ of Ho and Lu are 2.809 Å and 2.774 Å respectively. The solid lines are the variations of the lattice parameters predicted by elasticity theory and are discussed in the text.

To extract quantitative information from the longitudinal scans requires fitting a model to the data. The model used in our case was a modified form of the one developed by Fullerton *et al* [9] The main modifications we incorporated into our simulation programme were to allow for the presence of interdiffusion by writing the compositional profile as

a damped square wave, to include the form factors of the atoms [33], and to include the anomalous scattering factors [34]. This last modification was particularly important because of the proximity of the $Cu_{K\alpha 1}$ line to the L_{III} absorption edge of the rare earths. The salient parameters of this model are then: the number of lattice planes N_A and N_B, and their respective variances ω_A and ω_B; the lattice parameters d_A and d_B, and the continuous disorder δ; and interdiffusion σ, which is the width for which the relative concentration of material A lies between 0.8 and 0.2. Typical fits of this model to our data are represented by the solid lines in figure 3 and figure 4, where it can be seen that the model gives an excellent description of the data over nearly four decades of intensity. The parameters extracted from the fitting procedure are given in table 2, and displayed graphically in figures 5 and 6.

Table 2. The roughness amplitude A and exponent α determined from modelling the transverse Bragg peak line shapes of Ho/Lu and Ho/Y superlattices. For Ho_{16}/Y_{61} two values are given for these parameters corresponding to two orthogonal orientations of the sample around the surface normal; the measured substrate off-cut angle is given in parentheses. We estimate that the uncertainty in the value of α is ± 0.05.

Sample	Amplitude A	Exponent α
$(Ho_{44}/Lu_{16})_{50}$	0.020	0.95
$(Ho_{20}/Lu_{17})_{50}$	0.049	0.85
$(Ho_{8}/Lu_{18})_{75}$	0.019	0.87
$(Ho_{18}/Lu_{10})_{50}$	0.044	0.79
$(Ho_{12}/Lu_{34})_{32}$	0.037	0.86
$(Ho_{18}/Lu_{5})_{50}$	0.034	0.83
$(Ho_{24}/Lu_{14})_{50}$	0.050	0.78
$(Ho_{16}/Y_{61})_{50}$ (0.8°)	0.012	0.89
$(Ho_{16}/Y_{61})_{50}$ (0.1°)	0.002	0.86
$(Ho_{8}/Y_{30})_{30}$	0.028	0.81

4.2. Transverse scans

As a representative data set, we show in figure 7 a series of transverse scans through the superlattice reflections around (002) from sample Ho_{16}/Y_{61}. Attempts were made to fit the unusual line shape of the scattering with a single peak function. The best description of the data was found using a Lorentzian raised to the power of 5/2, which we write as

$$I(p_x) = \frac{I_0}{(1 + (p_x/\kappa)^2)^{5/2}} \tag{3}$$

where I_0 is the amplitude, and the FWHM is related to the inverse correlation length κ by FWHM = 1.131κ. In this initial fitting procedure no allowance was made for the finite resolution of the instrument. The widths (FWHM) of the scattering as a function of n extracted from such fits are displayed in figure 8, where it can be seen that they are approximately proportional to the index n, and hence to the reduced wave-vector q parallel to the growth direction. To investigate whether the line shape was isotropic in the plane of the film, we rotated the sample by 90° around [001] and repeated the same scans. The line shape itself was found to be insensitive to orientation, but the widths showed a pronounced anisotropy (figure 8). As a final check we also measured the broadening of the superlattice reflections around the (004) peak. It is evident in figure 8 that, for a given orientation of

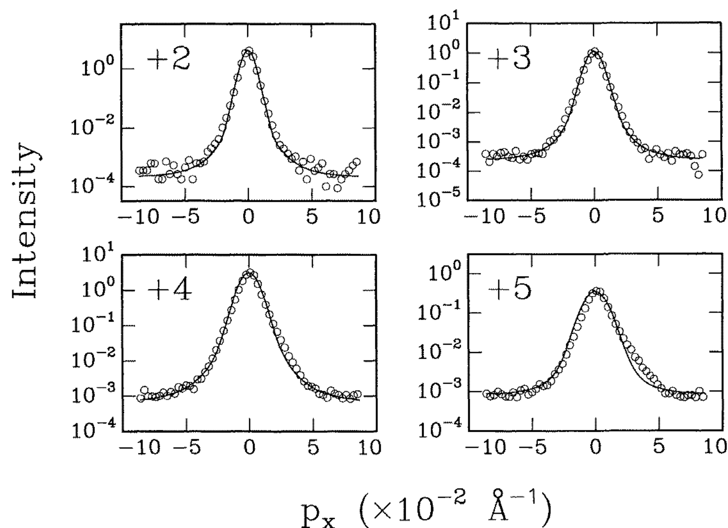

Figure 7. The x-ray scattering observed in transverse scans through four superlattice satellites of $(Ho_{16}/Y_{61})_{50}$. The solid line represents the result of a simultaneous least-squares fit of (2), convoluted over the mosaic distribution of the sample and the out-of-plane resolution. The values of the roughness amplitude A and exponent α derived from this fit are given in table 1. Note: an arbitrary scale factor has been used to normalize the spectra.

the sample, the satellites around the (002) and (004) peaks broaden at the same rate as a function of q.

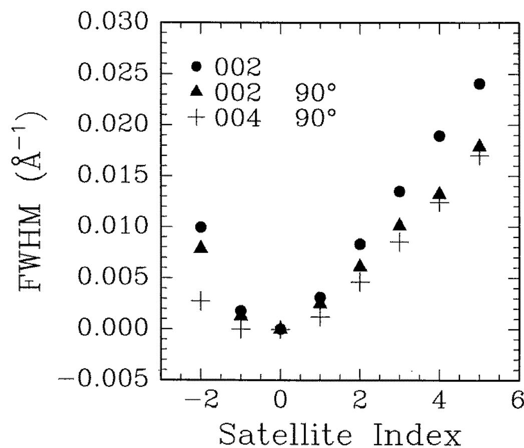

Figure 8. The measured increase in the width (FWHM) of the superlattice satellite reflections of Ho_{16}/Y_{61} around 002 (mounted in the (h0ℓ) plane and rotated by 90°) and 004 as a function of satellite index.

Less exhaustive scattering experiments were performed on all of the superlattices and yielded qualitatively similar results: the peaks broadened approximately linearly with q, and had a line shape that followed closely a Lorentzian to the 5/2. The sole exception to this

was sample Ho_{44}/Lu_{16}, where some of the satellites displayed a pronounced two-component line shape as shown in figure 9.

4.3. Dependence on growth temperature

In figure 10 we present the results of longitudinal scans from two of the nominally identical superlattices grown at substrate temperatures of 400, and 600 °C (the results from the sample grown at 250 °C are not shown for reasons of clarity). The first thing to note is that the samples do not have exactly the same bi-layer repeat length. Second, there are additional features evident that arise from interference between either the cap or substrate and the superlattice. Because of time limitations, this series was grown with only fifteen bi-layer repeats and this explains why these features are more evident than in the samples with fifty or more repeats. These features mean that we cannot fit the data using the model described earlier, and so we shall restrict ourselves to qualitative comments only. It is apparent that the higher-order satellites are more suppressed at elevated growth temperatures, presumably as the surface mobility is enhanced and hence the interdiffusion greater.

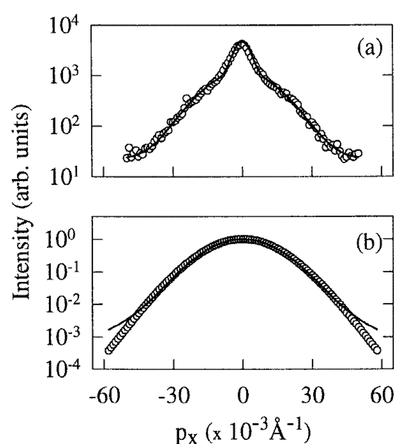

Figure 9. Transverse scan through the +2 superlattice peak of $(Ho_{44}/Lu_{16})_{50}$ showing (a) a two component line shape, and (b) a fit to the broad component after the central Gaussian peak was subtracted. The solid line in (b) is the result of a fit of the model described in the text.

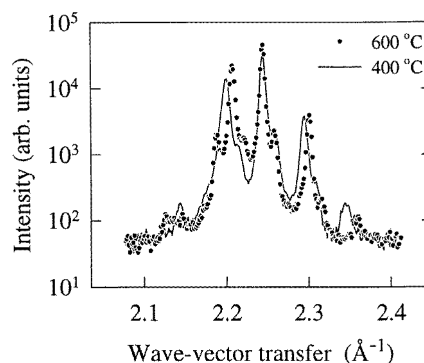

Figure 10. The x-ray scattering from two Ho/Y superlattices grown at substrate temperatures of 600 °C and 400 °C observed for a scan of the wave-vector transfer along [00ℓ]. The solid line is a fit to the model described in the text. The intensity at each value of ℓ was integrated by performing a scan normal to the [00ℓ] direction, as described in the text. The solid line is a fit to the model described in the text.

The transverse scattering was also investigated in this series, and in figure 11 we give a comparison of the observed line shape of the first superlattice satellite. As the substrate temperature is decreased the width of the peak steadily increases.

5. Discussion

We shall begin this section by considering the longitudinal data. The parameters describing the discrete cumulative roughness are displayed in figure 5 from which it can seen that there is a clear trend for the roughness to increase with the number of atomic planes in

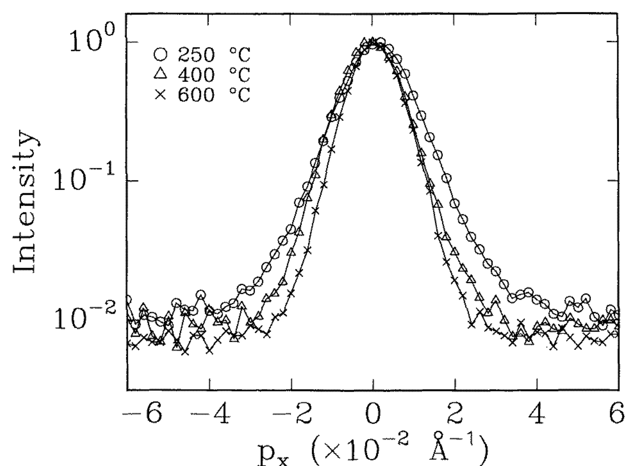

Figure 11. The dependence of the transverse line shape of the first superlattice satellite on the substrate temperature for three superlattices of nominal structure $(Ho_{40}/Y_{15})_{15}$.

both the Ho/Lu and Ho/Y systems. This finding is in accordance with what is expected for discrete cumulative roughness [9]. As this type of roughness results from limited atomic surface mobility, and, up to the point where it saturates, should scale as a function of the individual block lengths. Our data appears to be more consistent with the discrete cumulative roughness increasing as the square-root of the number of planes than a linear variation, as shown in figure 5, but the scatter of the data restricts us from proving this conclusively.

The inter-planar lattice spacing for the Ho/Lu system are shown in figure 6, and again a systematic trend is apparent, with the Ho and Lu tending to their bulk values as their fraction increases. The solid lines shown in figure 6 have been calculated from elasticity theory, using the elastic constants given in [36], and by assuming that the seed layer on which the superlattices are grown has a negligible influence. From the good agreement between our data and the calculations, this assumption would appear to be valid. From table 1 it can be seen that the parameter δ describing the continuous cumulative roughness, is approximately given by the difference in the average lattice parameters of the constituents as expected. One important aspect of the results presented in table 1 is that the derived values for the interface width are significantly lower than values in the range four to five lattice planes [6, 31] previously reported for similar systems. In these earlier studies the whole of the reduction in satellite intensity with increasing order was attributed entirely to interdiffusion, whereas our work has established that a significant factor in this reduction is the existence of discrete cumulative disorder.

The results from the transverse scans are now considered. On the basis of equation (2) it would appear that the interfaces in the rare-earth superlattices are rough with a value of the roughness exponent α between 1/2 and 1. The fact that a single-component line shape is observed instead of the sum of a diffuse and resolution limited peak may be because of the non-zero mosaic distribution of the sample, which was typically 0.25°. This means that the results are not sensitive to the roughness for distances r of more than $\approx$150 Å. Our results therefore suggest that for most of the samples L (see equation (1)) is larger than this size. To allow a simultaneous analysis of the line shape and its dependence on q we

performed a two-dimensional convolution of equation (2) over the approximately Gaussian mosaic distribution of the sample and the out-of-plane resolution of the instrument. A least-squares fit was then performed, comparing the model function to all of the transverse scans from one sample to determine the values of α and A. Apart from a background, the only parameter that was allowed to vary between different scans from the same sample was the intensity of each peak which is affected by other factors such as the degree of inter-diffusion. The solid lines through the data points in figure 7 represent the results of this fitting procedure. It can be seen that the model provides an excellent description of the data, both as a function of wave-vector transfer and satellite index. The value of α extracted for each of the superlattices investigated is given in table 2, and has an average of 0.85 ± 0.05. For the sample that displayed the two-component line shape (see figure 9) a slightly different analysis was used. In this case each superlattice peak was fitted to the sum of a Gaussian of the same width as the central peak, and a Lorentzian raised to a higher power. The Lorentzian component was then fitted directly to equation (2), correcting only for the vertical resolution. The parameters derived from the fit were $\alpha = 0.90$, and $A = 0.02$, in good agreement with the values given in table 2. Thus although we do not know why this sample displayed both the specular and non-specular components, the value of α extracted from the latter component is consistent with the values of α obtained from all of the other samples.

For Ho_{16}/Y_{61} two sets of values of the fit parameters are quoted for the two orientations of the sample investigated, along with the corresponding measured off-cut angle of the sapphire substrate. There is a marked correlation between the magnitude of the off-cut angle, which can be directly related to the terrace length on the substrate (see, for example, [35]), and the roughness: the orientation with the largest off-cut, and hence the smallest terraces, produces a rougher interface.

For the three samples fabricated at different growth temperatures we have also fitted the data shown in figure 11 using the method outlined above. The observed changes in the line shape as the substrate temperature is decreased correspond to an increase in the amplitude A from 0.008 to 0.019 and a concomitant increase in α from 0.83 to 0.93, as given in table 3. This is a very clear demonstration of the role of substrate temperature in determining the interfacial morphology. As the substrate temperature is reduced, atomic surface mobility becomes increasingly restricted. The ability to find sites of high co-ordination number is limited and the interface roughness increases.

Table 3. The dependence of the roughness amplitude A and exponent α on substrate temperature for a series of $(Ho_{40}/Y_{15})_{15}$ superlattices.

Growth Temperature (°C)	Amplitude A	Exponent α
250	0.019	0.93
400	0.022	0.87
600	0.008	0.83

We end by noting that the division made in this paper of the x-ray experiment into considerations of longitudinal and transverse scans is to a large extent artificial, and results from the fact that to date it has not yet proved possible to construct a model that gives a full description of the scattering from a superlattice. On the one hand the model due to Fullerton *et al* [9] cannot be rigorously applied to systems with conformal interfaces,

and on the other hand methods that have been developed to describe conformal roughness cannot be rigorously applied to systems with cumulative disorder. Most real systems will have both conformal and cumulative roughness, and there is a clear need for a model to be developed that can describe such systems.

6. Summary

In summary, we have performed a systematic study of the x-ray scattering from a series of rare-earth superlattices. From this work a more detailed picture of the overall structure has emerged. The longitudinal scans are well described by the kinematical scattering model due to Fullerton *et al.* [9], and this reveals that there is a significant degree of discrete cumulative disorder that increases with the thickness of the bi-layer. Evidence is also found for a residual interdiffusion extending over approximately three atomic planes. From an analysis of the transverse line shape of the superlattice reflections we determine the roughness exponent α to be 0.85 ± 0.05. This value is close to one and indicates that the interfaces in rare-earth superlattices are smooth, because as α tends to zero the interfaces become extremely jagged (see, for example, Schlomka *et al* [37] and Krim and Indekeu [38]). We also believe that this value indicates a conservative growth mode. Due to uncertainties in current theories it is not possible at this stage to draw any further conclusions from its value. We have also shown that x-ray scattering does provide reliable information on the interfacial roughness in MBE growth, and we suggest that the roughness exponent depends on the growth parameters, at least for length scales up to ≈ 150 Å.

This study also demonstrates that it is possible to obtain information on the interfaces using high-angle diffraction, which not only reduces the sensitivity to oxidized over layers, but also avoids complications arising from dynamical diffraction effects at low angle [10].

Acknowledgments

We would like to thank Doon Gibbs for his assistance with the experiments, and Robert Feidenhans'l for useful discussions. Beam line X22 is supported by the US DOE under Contract Number DE-AC0276CH00016. This work was supported by a grant from the Science and Engineering Research Council.

References

[1] Bauer E G *et al* 1990 *J. Mater. Res.* **5** 852
[2] Fullerton E E, Pearson J, Sowers C H, Bader S D, Wu X Z and Sinha S K 1993 *Phys. Rev.* B **48** 17432
[3] Kelly D M, Schuller I K, Korenivsk V, Rao K V, Larsen K K, Bottiger J, Gyorgy E M and van Dover R B 1994 *Phys. Rev* B **50** 3481
[4] Belien P, Schad R, Potter C D, Verbanck G, Moshchalkov V V and Bruynseraede Y 1994 *Phys. Rev.* B **50** 9957
[5] Family F 1990 *Physica* A **168** 561
[6] Majkrzak C F, Kwo J, Hong M, Yafet Y, Gibbs D, Chien C L and Bohr J 1991 *Advances in Physics* **40** 99
[7] Swaddling P P, McMorrow D F, Cowley R A, Ward R C C and Wells M R 1994 Phys. Rev. Lett. **73** 2232
[8] McWhan D B 1985 *Synthetic Modulated Structures* ed Chang L L and Giessen B C (New York: Academic)
[9] Fullerton E E, Schuller I K, Vanderstraeten H and Bruynseraede Y 1992 *Phys. Rev.* B **45** 9292
[10] Sinha S K, Sirota E B, Garoff S and Stanely H B 1988 *Phys. Rev.* B **38** 2297
[11] Cowley R A 1992 *Equilibrium Structure and Properties of Surfaces and interfaces* ed A Gonis and G M Stocks (New York: Plenum)
[12] Holy V and Baumbach T 1992 *Phys. Rev.* B **49** 10668
[13] Sinha S K 1994 *J. Physique* III **4** 1543

[14] Wolf D and Villain J 1990 *Europhys. Lett.* **13** 389
[15] Das Sarma S and Ghaisas S V 1992 *Phys. Rev. Lett.* **69** 3762
[16] Kardar M, Parisi G and Zhang Y C 1986 *Phys. Rev Lett.* **56** 889
[17] Das Sarma S and Tamborenea P 1991 *Phys. Rev. Lett.* **66** 325
[18] Lai Z W and Das Sarma S 1991 *Phys. Rev. Lett.* **66** 2348
[19] Hong Yan 1992 *Phys. Rev. Lett.* **68** 3048
[20] Kessler D A, Levine H and Sander L M 1992 *Phys. Rev. Lett.* **69** 100
[21] Iwamoto A, Yoshinobu T and Iwasaki H 1994 *Phys Rev. Lett.* **72** 4025
[22] Tong W M, Williams R S, Yanase A, Segawa Y and Anderson M S 1994 *Phys. Rev. Lett.* **72** 3374
[23] Yan X and Egami T 1993 *Phys. Rev.* B **47** 2362
[24] Chiarello R, Panella V, Krim J and Thompson C 1991 *Phys. Rev. Lett.* **67** 3408
[25] Thompson C, Palasantzas G, Feng Y P, Sinha S K and Krim J 1994 *Phys. Rev.* B **49** 4902
[26] Geer R E, Shashidhar R, Thibodeaux A F and Duran R S 1993 *Phys. Rev. Lett.* **71** 1391
[27] Sanyal M K, Sinha S K, Gibaud A, Satija S K, Majkrzak C F and Homa H 1992 *Surface X-ray and Neutron Scattering* ed H Zabel and I K Robinson (Berlin: Springer)
[28] He Y L, Yang H N, Lu T M and Wang G G *Phys. Rev. Lett.* **69** 3770
[29] Krim J, Heyvaert I, Van Haesendonck C and Bruynseraede Y 1993 *Phys. Rev. Lett.* **70** 57
[30] Kwo J, Gyorgy E M, McWhan D B, Disalvo F J, Vettier C and Bower J E 1985 *Phys. Rev. Lett.* **55** 1402
[31] Jehan D A, McMorrow D F, Cowley R A, Wells M R, Ward R C C, Hagman N and Clausen K N 1993 *Phys. Rev.* B **48** 5594
[32] Swaddling P P, McMorrow D F, Simpson J A, Wells M R, Ward R C C, Clausen K N 1993 *J. Phys.: Condensed Matter* **5** L481
[33] 1974 Ibers J A and Hamilton W C (ed) *The international table for X-ray Crystallography* Vol IV (Birmingham: Kynoch) p 101
[34] Satoshi Sasaki 1989 *KEK Report* No. 88-14 1989 (National Laboratory for high energy physics, Japan)
[35] Gibaud A, Cowley R A, McMorrow D F, Ward R C C and Wells M R *Phys. Rev.* B **48** 14463
[36] Scott T E 1995 *Handbook on the Physics and Chemistry of the Rare Earths, Volume 1* ed K A Gschneider Jr and L Eyring (Amsterdam: North Holland) p 591
[37] Schlomka J P, Tolan M, Schwalowsky L, Seeck O H, Stettner J and Press W 1995 *Phys. Rev.* B **51** 2311
[38] Krim J and Indekeu J O 1993 *Phys. Rev.* B **48** 1576